Combustion noise modeling using compressible simulations

By A. L. Birbaud AND H. Pitsch

1. Motivation and objectives

The objective of the present study is to assess the role of direct and indirect noise generated by the unsteady heat release in aircraft engines. Previous studies indicated that noise computations require numerical schemes of high-order accuracy to resolve the high-frequency components of the noise spectrum. In order to be able to predict these high-frequency components, a fully compressible reactive flow solver with a fourth-order space and time discretization has been developed on structured grids. In the present study, the general method is first presented. Then, some additional features are described, which are necessary to perform accurate simulations of realistic configurations.

2. Numerical approach

In a previous study, two solvers have been compared on a 1-D test case to assess their capability to compute the propagation of high-frequency acoustic waves (Birbaud & Pitsch 2007). It was shown that fourth-order accurate methods were more suited to compute these high-frequency components. In order to be able to increase both spatial and temporal discretizations, a density-based flow solver with an explicit Runge-Kutta time integration has been considered.

2.1. *Governing equations*

The general form used for the set of equations is the conservative form:

$$\frac{\partial \phi}{\partial t} + \frac{\partial \Phi}{\partial x_j} = s. \tag{2.1}$$

The vector ϕ is the vector of the conserved variables. In the following, the combustion model is based on the Flamelet Progress Variable approach by Pierce & Moin (2004). In this context, the balance equations for the conserved variables, the continuity, momentum, mixture fraction, progress variable and energy read:

$$\frac{\partial \rho}{\partial t} + \frac{\partial \rho u_j}{\partial x_j} = 0, \tag{2.2}$$

$$\frac{\partial \rho u_i}{\partial t} + \frac{\partial \rho u_i u_j}{\partial x_j} = \frac{\partial}{\partial x_j}\left(\tau_{ij} - p\delta_{ij}\right), \tag{2.3}$$

$$\frac{\partial \rho z}{\partial t} + \frac{\partial \rho u_j z}{\partial x_j} = \frac{\partial}{\partial x_j}\left(\rho D \frac{\partial z}{\partial x_j}\right), \tag{2.4}$$

$$\frac{\partial \rho c}{\partial t} + \frac{\partial \rho u_j c}{\partial x_j} = \frac{\partial}{\partial x_j}\left(\rho D \frac{\partial c}{\partial x_j}\right) + \rho \omega_c, \tag{2.5}$$

$$\frac{\partial \rho E}{\partial t} + \frac{\partial \rho u_j E}{\partial x_j} = -\frac{\partial q_j}{\partial x_j} + \frac{\partial}{\partial x_i}\left[\left(\tau_{ij} - p\delta_{ij}\right) u_j\right]. \tag{2.6}$$

for a multi-component reactive flow $\phi = \{\rho, \rho u, \rho v, \rho w, \rho z, \rho c, \rho E\}^T$, where z, c and E are the mixture fraction, progress variable and total energy, including chemical energy, respectively. E is expressed by $E = h - p/\rho + 1/2 u_i u_i$, where h refers to the total enthalpy. In the energy equation, q_j, the enthalpy flux is defined by $q_j = -\lambda \partial T/\partial x_j + \rho \sum_{k=1}^{k=N} h_k Y_k V_{k,j}$. The $V_{k,j}$ are the diffusion velocities. The viscous tensors are defined by $\tau_{ij} = -2/3\mu(\partial u_k/\partial x_k)\delta_{ij} + \mu(\partial u_i/\partial x_j + \partial u_j/\partial x_i)$. The total enthalpy, h, is defined as:

$$h = h_s + \sum_{k=1}^{k=N} \Delta h^0_{f,k} Y_k, \tag{2.7}$$

To close the above system of equations, two more equations of state are needed to obtain the temperature and the pressure. We use the equation of state for the sensible enthalpy and the ideal gas equation of state to close the system:

$$h_{s,k}(T) = \int_{T_o}^{T} C_{p,k}(T^*) dT^*. \tag{2.8}$$

$$P = \rho R T \sum_{k=1}^{k=N} \frac{Y_k}{W_k}. \tag{2.9}$$

Many different forms of the energy equation can be used for compressible simulations. In the literature, some authors derive an equation for the pressure (Pantano, Sarkar & Williams 2002), the temperature, or the sensible energy (Pantano & Pullin 2003). Transporting the pressure can be interesting to avoid errors due to its reconstruction. However, this does not guarantee the conservation of energy. In the present study, we use the total chemical energy. In this case, the chemical source term does not appear explicitly in the energy equation, but is contained in the total enthalpy (Poinsot & Veynante 2005). A time step is organized as follows: The conserved variables are first advanced by the scheme. Once the density, mixture fraction, momentum and energy are known, the primitive variables are calculated. The species mass fractions are used along with polynomial laws and the computed total enthalpy to recompute the temperature by an iterative method. Once the temperature is known, the pressure is obtained by solving the ideal gas equation of state.

It is interesting to examine how the system is coupled, compared to an approach where the species mass fractions are transported. In the latter case, as the density can directly be obtained by the summation of all the ρY_k, a perturbation of the mixture directly generates perturbations of density. If the time integration is explicit, as the temperature is a function of energy and mixture, it will also see the mixture perturbation. The pressure, reconstructed using the updated variables that have the modification, will be directly affected through ρ, W and T. We have a $\rho - T - W - P$ coupling (W refers to the mixture molar mass):

$$\frac{d\rho}{\rho} \sim -\frac{dT}{T} + \frac{dP}{P} + \frac{dW}{W}. \tag{2.10}$$

When the species mass fractions are not transported, the coupling mechanism is modified. Instead of ρY_k, the mixture fraction accounts for the mixing, and is no more directly coupled to the density. For example, a fluctuation of the mixture fraction will affect first the quantities obtained from the chemical table, in our case, the species mass fractions. As a consequence, this change will affect the temperature, through the total enthalpy. Then the pressure is also affected, through the equation of state. Finally, the coupling with the density is achieved through the velocity that contains the effect of the pressure gradient on the field. In this situation, we have a $P - T - W$ coupling:

$$\frac{dP}{P} \sim \frac{dT}{T} - \frac{dW}{W}. \tag{2.11}$$

Hence, a perturbation of the temperature can generate a strong pressure fluctuation, keeping the density constant, at a given time step. This simple analysis shows that the response of the flow solver to a change in composition is very sensitive to the way the mixture fraction and density are coupled.

2.2. *Boundary conditions*

The boundary condition makes use of the characteristic form of the Navier-Stokes equations proposed by Thompson (1987). The 1-D relations have been described by Poinsot & Lele (1992), and more recently, with the 3-D terms included by Lodato, Domingo & Vervisch (2008). The waves for velocity, density, and temperature follow the classical form found in these papers. The waves imposed on the mixture fraction and progress variable are those of a scalar, based on a convective time scale. For example, if we consider a subsonic boundary condition, and either the mixture fraction or progress variable and the energy, we have:

$$\frac{\partial \rho Z}{\partial t} = \rho \frac{\partial Z}{\partial t} + Z \frac{\partial \rho}{\partial t}, \tag{2.12}$$

$$\frac{\partial \rho E}{\partial t} = \rho \frac{\partial E}{\partial t} + E \frac{\partial \rho}{\partial t}. \tag{2.13}$$

Using the waves computed for the density, and the waves imposed on the mixture fraction, gives the boundary condition for Z. The same procedure is applied to compute the waves for the energy equation; with $dh = C_p dT$, one obtains:

$$\frac{\partial \rho E}{\partial t} = \frac{\partial}{\partial t}\left(\rho h - p + \frac{1}{2}\rho u_i u_i\right), \tag{2.14}$$

$$= \rho C_p \frac{\partial T}{\partial t} + h \frac{\partial \rho}{\partial t} - \frac{\partial p}{\partial t} + \frac{1}{2} u_i u_i \frac{\partial \rho}{\partial t} + \rho \left(u \frac{\partial u}{\partial t} + v \frac{\partial v}{\partial t} + w \frac{\partial w}{\partial t}\right). \tag{2.15}$$

Once the waves for density, velocity and temperature are known, Eq. (2.15) gives the condition to be imposed on the total energy. This 3-D approach has been tested successfully on 2-D test cases, not shown in this study, where a pressure pulse is initialized in the middle of the domain. With the fourth-order scheme, the amplitude of the reflected wave is around 3 %.

3. Results

3.1. *Sound emitted by a pair of co-rotating vortices*

In order to test the accuracy of the solver, the sound emitted by two co-rotating vortices is computed. The vortices, of radius r_c, are separated by a distance of $2r_0$, as shown in

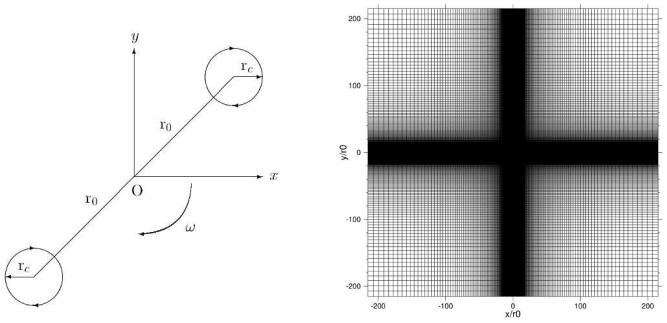

FIGURE 1. Dual vortices test case. Left: Schematic view of the configuration. Right: 2-D mesh.

Fig. 1 (left). In this case, the rotation Mach number (M_r) is based on the maximum rotation velocity, $M = \Gamma/(4\pi r_c c_0) = 0.5$, and $M_r(r_0) = 1/9$. The speed of sound is set to $c_0 = 346$ m/s, and $r_c = 7.92\times10^{-4}$ m, which is the distance from the center of each vortex at which the velocity is maximum. The domain size of the simulation is 1.4 m$\times$1.4 m. The period of rotation of the two vortices around each other is given by $T_r = 8\pi^2 r_0^2/\Gamma$. The system formed by the two vortices behaves like an acoustic quadrupole with a frequency equal to $f = 2f_r$. With $M = 0.5$, one obtains f=3365 Hz. The domain is discretized by 489 $\times$ 489 points, and the mesh is refined in the vicinity of the vortices as shown in Fig. 1 (right). This configuration has been studied by several authors. Direct Numerical Simulations of the sound radiated by the co-rotating vortices have been performed for different rotation Mach numbers by Mitchell *et al.* (1999), and the case corresponding to $M = 0.5$ has been investigated by Bogey, Bailly & Juve (2002). They have shown that after a given number of rotations, the two vortices collapse, and characterized the sound emitted during this transient phenomenon. An analytic solution for the acoustic pressure evolution in the limit case of point vortices has also been derived by Moehring (1978). Mitchell *et al.* (1999) extended this analysis to viscous vortices. Equation (3.1) provides an analytical expression for the pressure perturbation:

$$p'(r,\theta,t) = -\frac{\rho_0\Gamma^4}{64\pi^3 r_0^4 c_0^2}\left(J_2\left(\frac{2\Omega_0 r}{c_0}\right) sin(2\theta + 2\Omega_0 t) + Y_2\left(\frac{2\Omega_0 r}{c_0}\right) cos(2\theta + 2\Omega_0 t)\right). \tag{3.1}$$

where J_2 and Y_2 refer to the first and second kind of Bessel functions, respectively, and $\Omega_0 = \Gamma/(4\pi r_0^2)$ is the rate of rotation of the vortex pair. The pressure signal has been recorded at 50 r_0 in $x-$ and $y-$ directions. This corresponds to $r/\lambda \simeq 0.55$. Figure 2 shows a snapshot of the instantaneous acoustic pressure. The characteristic spiral pattern is qualitatively well-captured by the solver. Figure 3 shows a quantitative comparison of the pressure time signals obtained at an angle of 45^o off the axis with Eq. (3.1), and the simulation results. Data shown in Fig. 3 indicate that a reasonable agreement with the analytical expression is obtained. The difference in the signal amplitude is attributed to the use of the spatial filtering. In order to eliminate the transient due to the initialization, the filter amplitude is set to a high value, then decreased. On a transient phenomenon, this strategy might affect to a certain extent the results, but it is helpful to prevent the non-resolved part from perturbing the pressure field.

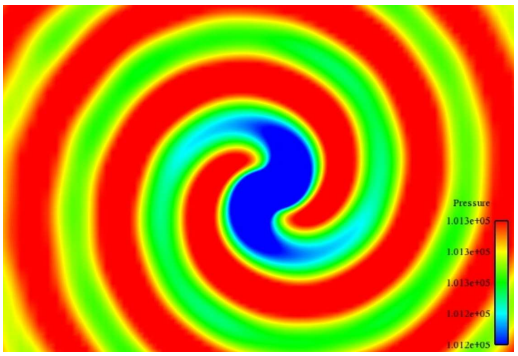

FIGURE 2. Snapshot of the pressure field illustrating the quadrupole spiral pattern.

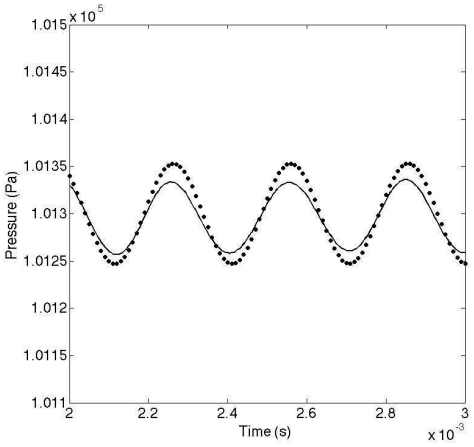

FIGURE 3. Pressure traces at $r/\lambda = 0.55$, with an angle of 45^o off the axis. Results of the simulation (———), analytical response obtained from Eq. (3.1) (•).

3.2. *The combustor case: Toward combustion noise simulations*

In this section, a more realistic case is considered. The geometry is shown in Fig. 4. It consists of a combustion chamber terminated by a diffuser placed at the end of an exhaust duct. The duct length is large compared to the combustion chamber length. The fuel and the air are injected separately and mix in the combustion chamber. A methane-air diffusion flame is stabilized in a central recirculation region. This geometry aims to reproduce the experiments performed by Bake *et al.* (2005). Power density spectra of the pressure signals recorded in the combustion chamber and in the exhaust duct indicate that the system oscillates at resonant frequency of 115 and 90 Hz, respectively.

In order to match the measurements' sound pressure levels, it is first interesting to examine very briefly the acoustic response of the system. The acoustic wavelength in the combustion chamber is based on the speed of sound in the hot products. With a typical length of 0.113 m, the resonant frequency f_r would be closer to 2000 Hertz for a longitudinal mode. This mode could also come from a Helmholtz resonator behavior of the combustion chamber plus the converging-diverging nozzle. In this case, f_r is computed using

FIGURE 4. Schematic view of the computed domain. The flow issued from the upstream swirlers is accounted for by imposing velocity profiles on the inlets. The combustion chamber length is $L_c = 0.113$ m, converging-diverging nozzle, 0.125 m and approximately 1 m.

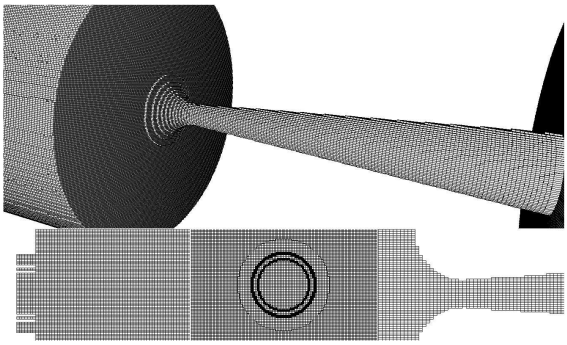

FIGURE 5. The 3-D structured mesh used for the simulations. Δy and Δz are kept constant and equal to $5\ 10^{-4}$ m.

an equivalent length L_e accounting for the mass inertia in the nozzle, $L_e = \int_0^1 S_e/S(x)dx$, where S_e is the surface at the exhaust (Hirschberg 2001). The resonant frequency is then given by:

$$f_r^2 = \frac{c^2 S_e}{4\pi^2 L_e V}. \tag{3.2}$$

where V is the combustion chamber volume and c is the speed of sound. One obtains f_r=151 Hz. This value is closer to that found in the experiments, but results indicate that the 115 Hz mode requires a more elaborate acoustic analysis to be clearly identified. From these observations, the computational domain is designed to capture the main physical mechanisms accounting for the noise components measured in the exhaust pipe. The upstream part of the combustion chamber is not computed, but to take into account the swirlers, velocity profiles are imposed, to satisfy the exhaust Mach number of 0.47. The mesh is 3-D cartesian and comprises 305 x 204 x 204 nodes. The velocity profiles at the inlet are imposed using characteristics. Schematic views of the domain and the mesh are shown in Figs. 4 and 5, respectively. Preliminary 2-D simulations have also been performed. In order to eliminate the influence of the non-resolved acoustic waves on the results, a spatial filter is applied on the conserved quantities at each time step. The filter used is the 9 points filter proposed by Bogey & Bailly (2004). The filter order is decreased in the vicinity of the walls, and near the injection region.

For the reactive flow, the chemistry tabulation is generated using the GRI 2.11 mechanism. At this point, the reactive full 3-D case is being investigated. First, the non-reactive flow including the mixture fraction is computed. Figure 6 shows an instantaneous view of the pressure and velocity fields after 3.4 ms. Preliminary results indicate that according

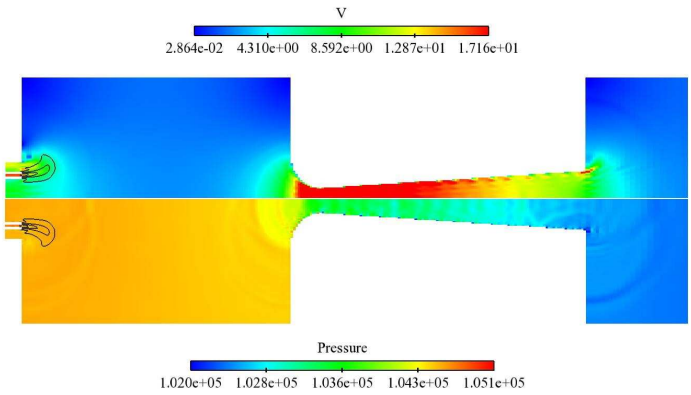

FIGURE 6. Snapshots of the velocity (top) and pressure (bottom) after 5.3 ms. Mixture fraction contours are superimposed, 2-D results.

to the previous remarks about the $P-T-W$ coupling, to avoid the generation of acoustic waves due to the slow density adaptation to mixture fluctutations, the mixture fraction is transported as a passive scalar until a statistically stationary mixing field has developed. Before igniting the flow, the density field is recomputed using chemistry tabulation. This avoids the generation of strong pressure oscillations in the domain, and is also currently being tested.

4. Conclusions and future work

In this study, a reactive compressible flow solver has been presented in order to simulate the noise radiated by the flame in a confined geometry. The scheme, boundary conditions and combustion model are described. A non-reactive verification test case is presented. A realistic validation test case is finally considered. Geometry and conditions are based on the geometry proposed by Bake *et al.* (2005). For this geometry, the non-reactive flow has been computed and the reactive case is presently considered. After the validation, the next step will be to examine on a fundamental level the generation of direct and indirect noise components in the combustion chamber.
Also, a Compressible Immersed Boundary Method, and a shock-capturing scheme, are being developed and may be added to the flow solver to extend its capability to complex subsonic and supersonic flows.

Acknowledgments

This work is supported by NASA. The authors gratefully acknowledge the helpful discussions with Dr. A. Giauque.

REFERENCES

BAKE, F., MICHEL, U., ROEHLE, I., RICHTER, C., THIELE, F., LIU, M. & NOLL, B. 2005 Indirect combustion noise generation in gas turbines. 11^{th} AIAA-CEAS Aeroacoustics Conference 23 - 25 May 2005, Monterey, California, 2005-2830.

Berglund, M. & Fureby, C. 2007 LES of supersonic combustion in a scramjet engine model. *Proc. Comb. Inst.* **31**, 2497–2504.

Birbaud, A. L. & Pitsch, H. 2007 Compressible solvers for combustion noise simulations. *Ann. Res. Briefs.*, 265–276.

Bogey, C. & Bailly, C. 2004 A family of low dispersive and low dissipative explicit schemes for flow and noise computations. *J. of Comp. Phys.* **194**, 194–214.

Bogey, C., Bailly, C. & Juve, D. 2002 Computation of flow noise using source terms in linearized Eulers equations. *AIAA J.* **40**(2), 235–243.

Hirschberg, A. 2001 Introduction to aero-acoustics of internal flow. *Advances in aeroacoustics, Lecture series.* March 12-16 Von Karman Institute, Belgium.

Lodato, G., Domingo, P. & Vervisch, L. 2008 Three dimensional boundary conditions for direct and large-eddy simulations of compressible viscous flows. *J. Comp. Phys.* **227**, 5105-5143.

Mitchell B. E., Lele S. K. & Moin P. 1995 Direct computation of the sound from a compressible co-rotating vortex pair. *J. Fluid Mech.* **285**, 181–202.

Moehring B. E. 1978 On vortex sound at low Mach number. *J. Fluid Mech.* **85**(4), 685–691.

Pantano, C., & Pullin D. I. 2003 Large eddy simulation of a turbulent reacting compressible jet using the stretched vortex subgrid model. 56^{th} APS Meeting, November 23-25., East Rutherford, N.J.

Pantano, C., Sarkar, S. & Williams, F. A. 2002 Mixing of a conserved scalar in a turbulent reacting shear layer. *J. Fluid. Mech.* **481**, 291–328.

Pierce, C. D. and Moin, P. 2004 Progress variable approach for large-eddy simulation of non-premixed turbulent combustion. *J. Fluid. Mech.* **504**, 73–97.

Poinsot, T. J. and Lele, S. K. 1992 Boundary conditions for direct simulations of compressible viscous flows. *J. Comp. Phys.* **101**, 104–129.

Poinsot, T. & Veynante, D. 2005 Theoretical and Numerical Combustion, 2^{nd} Edition, *Edwards.*

Thomspon, K. W. 1987 Time dependent boundary conditions for hyperbolic systems. *J. Comp. Phys.* **68**, 1–24.